Wiley Online Library
Early View publication on www.wileyonlinelibrary.com
(issue and page numbers not yet assigned;
citable using Digital Object Identifier – DOI)

J. Biophotonics 1–6 (2016) / **DOI** 10.1002/jbio.201500290

Journal of BIOPHOTONICS

FULL ARTICLE

Tunable fibre-coupled multiphoton microscopy with a negative curvature fibre

Ben Sherlock[*, 1], *Fei Yu*[2], *Jim Stone*[2], *Sean Warren*[1], *Carl Paterson*[1], *Mark A. A. Neil*[1], *Paul M. W. French*[1], *Jonathan Knight*[2], *and Chris Dunsby*[1, 3]

[1] Department of Physics, Imperial College London, London, SW7 2AZ, UK
[2] Department of Physics, University of Bath, Bath, BA2 7AY, UK
[3] Centre for Histopathology, Imperial College London, London, SW7 2AZ, UK

Received 9 November 2015, revised 20 January 2016, accepted 27 January 2016
Published online 15 March 2016

Key words: Photonic crystal fibre, negative curvature, multiphoton

Negative curvature fibre (NCF) guides light in its core by inhibiting the coupling of core and cladding modes. In this work, an NCF was designed and fabricated to transmit ultrashort optical pulses for multiphoton microscopy with low group velocity dispersion (GVD) at 800 nm. Its attenuation was measured to be <0.3 dB m^{-1} over the range 600–850 nm and the GVD was -180 ± 70 fs^2 m^{-1} at 800 nm. Using an average fibre output power of ~20 mW and pulse repetition rate of 80 MHz, the NCF enabled pulses with a duration of <200 fs to be transmitted through a length of 1.5 m of fibre over a tuning range of 180 nm without the need for dispersion compensation. In a 4 m fibre, temporal and spectral pulse widths were maintained to within 10% of low power values up to the maximum fibre output power achievable with the laser system used of 278 mW at 700 nm, 808 mW at 800 nm and 420 mW at 860 nm. When coupled to a multiphoton microscope, it enabled imaging of *ex vivo* tissue using excitation wavelengths from 740 nm to 860 nm without any need for adjustments to the set-up.

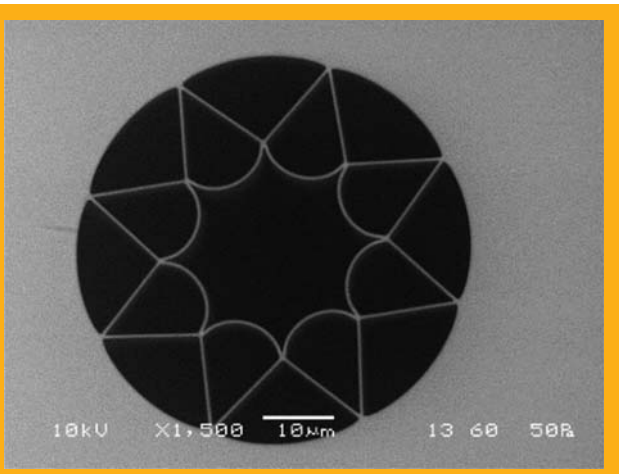

1. Introduction

Optical fibre is a key enabling technology for the development of high resolution, multimodal optical clinical imaging systems as it enables bulky and expensive components to be located away from the point of contact with the patient and therefore allows imaging devices to become more compact, robust and ergonomic. Nonlinear microscopy techniques such as two photon excited fluorescence microscopy and second harmonic microscopy (SHG) require ultrashort excitation pulses to be delivered to the sample. They therefore require optical fibres with low attenuation over a distance of several meters, low dispersion, guiding of light in a single spatial mode and the capability to deliver pulses with peak powers of several kW without significant temporal or spectral broadening and without physical

* Corresponding author: e-mail: b.sherlock@imperial.ac.uk

damage. For multiphoton microscopy, these requirements should ideally be met across an extended wavelength range to enable the efficient excitation of diverse fluorophores.

The first fibre-coupled nonlinear microscopes used conventional single-mode fibres with dispersion compensation schemes to combat the pulse broadening that occurred inside the fibre [1–3]. Although successful in demonstrating the proof-of-principle of fibre-coupled nonlinear microscopy, these early systems were hampered by self-phase modulation induced temporal and spectral broadening within the fibre. In 1999 the realization of photonic bandgap fibres (PBFs) [4] that guide light inside an air filled core provided a new approach for delivery of excitation light for fibre-coupled nonlinear microscopy. By guiding light so that it propagates mainly in air, these fibres suppress optical nonlinearity by several orders of magnitude, allowing microscopes and endoscopes to be constructed without complex dispersion compensation units [5–9]. Despite these advantages, however, PBFs are not well suited to broadband delivery of ultrashort pulses due to the narrow transmission bandwidth that is inherent to this guidance mechanism and the rapid change in group velocity dispersion (GVD) with wavelength that results from not being able to cancel waveguide dispersion using material dispersion [10]. Following the development of PBF, a new variety of hollow core photonic crystal fibre that employed a different guidance mechanism was introduced [11]. Inhibited coupling (IC) fibres do not possess an intrinsic bandgap but confine light by suppressing the overlap between core and cladding modes. These fibres can be implemented for visible and NIR radiation with flat dispersion curves and transmission bandwidths greater than 200 nm. The most well-known of the IC fibres are the hypocycloid core Kagome fibres that are used in the field of high power pulse delivery and nonlinear optics [12]. In 2014, an IC hollow core fibre was used with a multiphoton microscope to generate autofluorescence images of *ex vivo* human skin samples [13]. The GVD of the fibre used in this work, for pulses with a centre wavelength of 780 nm and a bandwidth of 90 nm was measured to be 150 $fs^2\ m^{-1}$. However, this fibre had an attenuation of 5.1 $dB\ m^{-1}$ and so would require a high power light source to deliver sufficient light at the fibre output, especially if lengths >1 m were employed.

In this paper, we present the optical characterization of an IC hollow core negative curvature fibre (NCF) with attenuation <0.3 $dB\ m^{-1}$ and dispersion values <1600 $fs^2\ m^{-1}$ across a bandwidth of 180 nm that is ideally suited for guiding ultrashort near infrared (NIR) pulses such as those used in nonlinear fluorescence microscopy [14]. We then demonstrate its application in multiphoton microscopy of unlabelled *ex vivo* mouse skin over a range of excitation wavelengths with no system adjustments other than the emission wavelength of the laser oscillator.

2. Negative curvature hollow core fibre

NCF is a simple hollow core fibre which is characterized by the inverted curvature of its core wall [15]. The NCF structure is shown in Figure 1. NCF exhibits very low attenuation at long wavelengths in the mid-infrared spectrum, with a minimum attenuation of 23.3 $dB\ km^{-1}$ measured at 2400 nm and 85 $dB\ km^{-1}$ at 4000 nm [16]. However, in the visible and near infrared part of the spectrum, the fibre performance is degraded by the difficulty of fabricating the smaller structures required and 'imperfection' loss starts to dominate the fibre attenuation, [15, 16].

The NCF in this paper was drawn with F300 fused silica material by a standard stack-and-draw method. A fluorine-doped silica tube was used as an external jacket in the final fibre draw. This jacket is found to reduce the attenuation of NCFs at short wavelengths. By using a fluorine-doped silica jacketing tube, we have previously demonstrated NCFs with greatly reduced attenuation 0.15 dB/m at 532 nm and 40 $dB\ km^{-1}$ at 1064 nm [17, 18]. We believe that the reduced viscosity of the doped glass compared to pure undoped silica enables the fibre to be drawn at a reduced temperature and thus a higher viscosity mitigating the degradation of cladding structure when NCFs are scaled to smaller sizes for shorter wavelengths. The NCF used in this paper had an air core inner diameter of 22 μm and the numerical aperture (NA) was experimentally determined to be 0.036 (measured at $1/e^2$ of the maximum intensity). This NA value compares favourably with the measured value (0.038) of a similar NCF with a slightly smaller inner diameter of 15 μm [17].

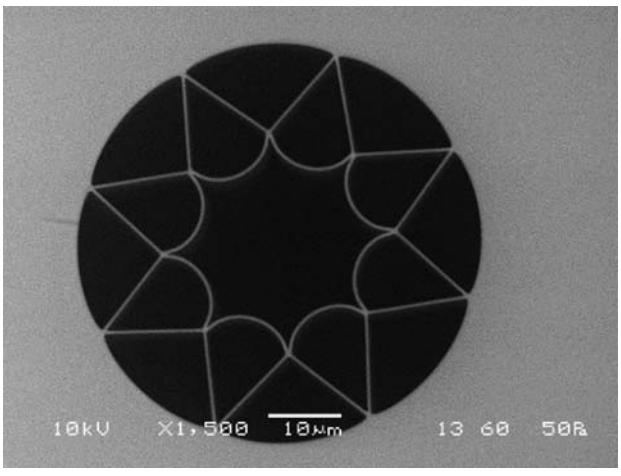

Figure 1 Scanning electron microscope image of the NCF.

3. Fibre characterization

To characterise the NCF for its application in nonlinear microscopy, the attenuation, pulse-length broadening and output mode profiles were measured as functions of wavelength. In addition, the spectral and temporal widths of pulses at the fibre output were recorded as functions of the average power to determine the influence that nonlinear processes in this fibre have on pulse propagation.

3.1 Attenuation

The optical attenuation spectrum was obtained by a cut-back experiment (fibre lengths of 43 m and 11 m were used) with a white light source (Tungsten lamp) and broadband spectrometer (Ando AQ-6315B). Free-space optics were used to couple into and out of the NCF and excitation of only the air core was ensured and continuously monitored by imaging the intensity distribution at the output end of the NCF. As shown in Figure 2 the fibre has a transmission band with a width of 250 nm from 600–850 nm that is well suited for nonlinear microscopy. Across this transmission band, the propagation loss was measured to be <0.3 dB m^{-1}. The high attenuation peaks at 850 nm and 900 nm are due to coupling between the guided mode of the hollow core and a cladding mode which is localized to a silica strut in the cladding. These spectral features arise because although these modes have very different dispersion curves their effective indices cross in this spectral range. In this work the bending loss was not measured for this fibre, however bending losses for a similar NCF are reported in a paper in which the authors observed no measurable bending loss for bend diameters down to 80 mm [17].

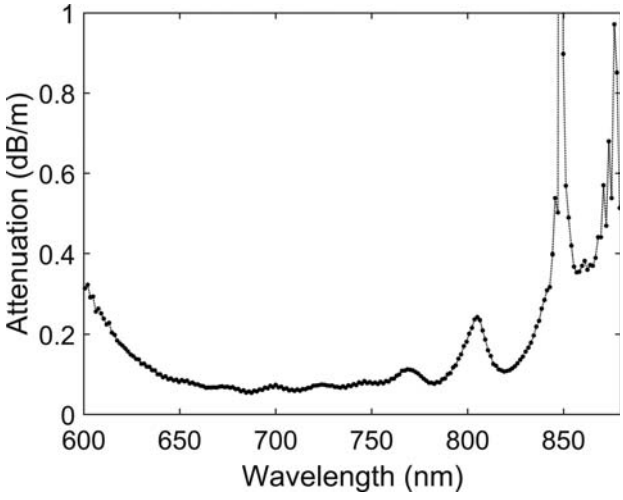

Figure 2 Attenuation of the NCF as measured by cut back experiment using a white light source.

3.2 Group velocity dispersion

The group velocity dispersion (GVD) was characterised using pulse width measurements acquired using an intensity autocorrelator (Femtochrome FR-103XL).

The mode-locked Ti:Sapphire laser (Spectra Physics Mai Tai HP) used in this work emits transform-limited sech-squared pulses with a measured temporal width of 87 ± 1 fs at 800 nm. The pulses are temporally broadened by dispersion occurring in both the bulk optics of the optical setup and the NCF. In order to separate the dispersion arising in the bulk optics from that of the NCF, the temporal pulse widths were measured after the light had propagated through the experimental setup with the NCF fibre removed (see Figure 3a). As is shown by the raw autocorrelator data in Figure 3c normal dispersion in the bulk optics broadens the temporal width of 800 nm pulses to 165 ± 1 fs. Measurements of the temporal pulse width following the introduction of 1.5 m of NCF into the beam path (Figure 3b) produced the result of 158 ± 2 fs indicating the fibre is weakly (anomalous) dispersive at this wavelength. The error on the autocorrelation measurements was estimated by taking the standard deviation of five repeat measurements. Pulse duration measurements following propagation along 1.5 m of hollow core photonic band gap fibre with zero GVD at 761 nm are included in Figure 3d for comparison. The GVD of the NCF was calculated using Eq. (1) (adapted from [19]) and plotted in Figure 3d,

$$\begin{aligned} \mathrm{GVD_{fibre}} &= (\mathrm{GDD_{total}} - \mathrm{GDD_{bulk}})/L \\ &= \frac{\tau_{\mathrm{in}}}{4L\ln 2}\left[\sqrt{(\tau_{\mathrm{total}}^2 - \tau_{\mathrm{in}}^2)} - \sqrt{(\tau_{\mathrm{bulk}}^2 - \tau_{\mathrm{in}}^2)}\right] \end{aligned} \quad (1)$$

where L is the fibre length, $\mathrm{GVD_{total}}$ is the total GVD of the fibre and the bulk optics and $\mathrm{GVD_{bulk}}$ is the GVD of the bulk optics alone and τ_{in}, τ_{bulk}, τ_{total} are the pulse durations measured directly at the laser output, after the pulses have passed through the bulk optics only and when the pulses have passed through the bulk optics and NCF respectively. At 800 nm the GVD of the fibre was found to be –180 ± 70 fs^2 m^{-1}. The error estimate for the GVD measured at 800 nm was obtained by performing 5 repeat autocorrelation measurements for each of τ_{in}, τ_{bulk}, and τ_{total}, and the error in GVD was then estimated using standard error propagation for

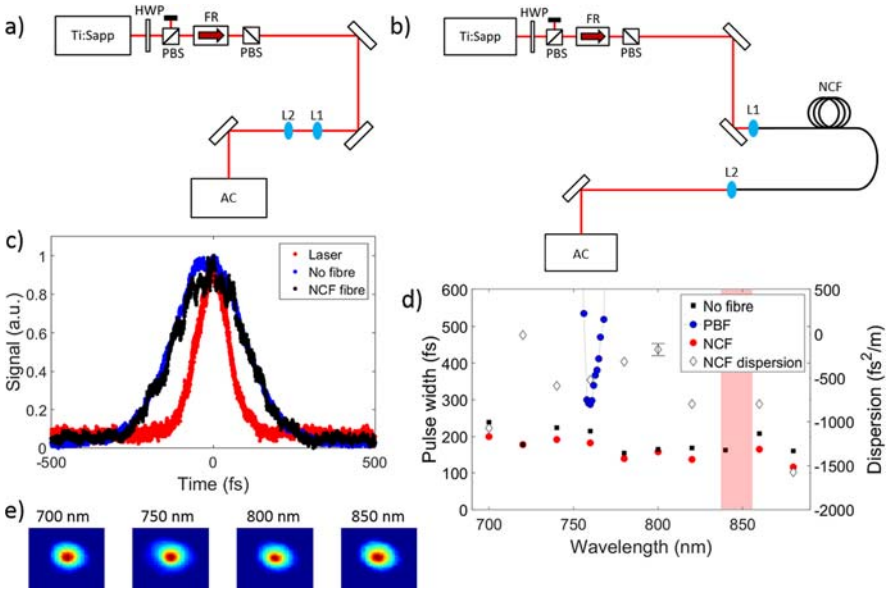

Figure 3 Schematic of the experimental setup used for measuring the temporal widths of pulses from a mode-locked Ti : Sapphire laser in the absence (**a**) and presence (**b**) of the negative curvature fibre. AC: Autocorrelator, FR: Faraday rotator; HWP: Half waveplate; L1 and L2: Fibre coupling lenses; NCF: Negative curvature fibre; PBS: Polarising beamsplitter. (**c**) Raw autocorrelator traces for 800 nm pulses originating directly from the laser (red), propagating through the power control and coupling optics (blue) and propagating through the optics and the NCF fibre (black). (**d**) Temporal pulse widths measured as a function of wavelength for femtosecond pulses propagating through power control and fibre coupling optics only (black), a 1.5 m hollow core photonic band gap fibre (blue) and 1.5 m of NCF (red). On the right hand *y*-axis, the dispersion for the NCF fibre is plotted as a function of wavelength (white diamonds). All pulse widths were measured using 20 mW average optical power at the autocorrelator. The red shaded spectral region corresponds with the core-cladding resonance around 850 nm shown in Figure 1. (**e**) Spatial profile of the NCF single mode output recorded at four wavelengths.

Eq. (1). Therefore, error bars are only shown in Figure 3d for this wavelength: we would expect the error bars at other wavelengths to be of a similar magnitude.

A CCD camera (Ximea MQ013CG-ON) was used to record the beam profile at the output of the NCF in order to analyse the modal distribution of the light exiting the fibre. The absence of modal cut-offs in NCF mean that across the transmission band, higher order modes are also supported and propagate along the fibre albeit with much higher loss than the fundamental mode [20]. Whenever we used

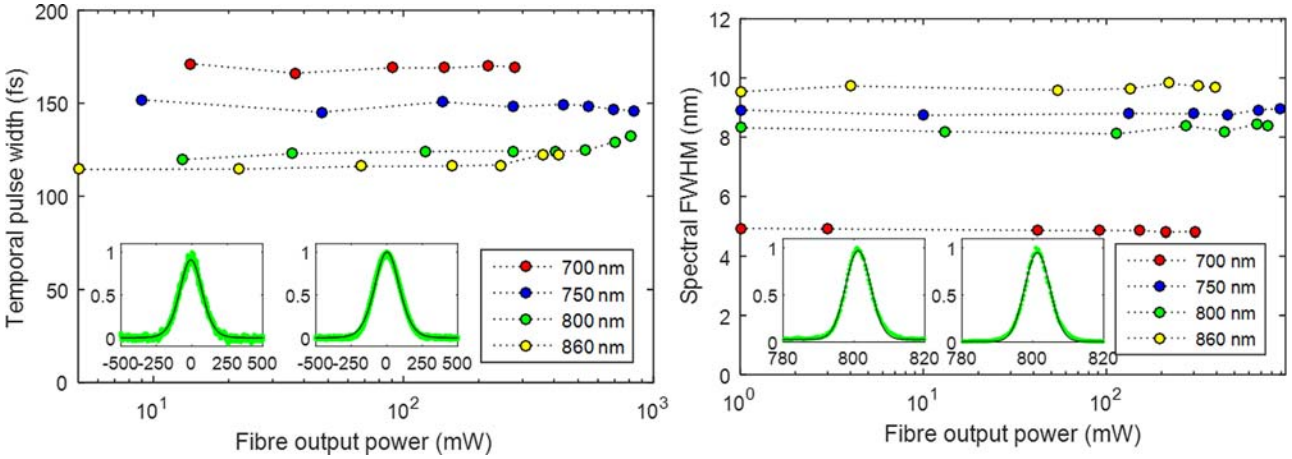

Figure 4 (**Left**) Temporal output pulse width variation with average output power. Insets show raw autocorrelator traces at 800 nm at 20 mW (**left**) and 520 mW (**right**) average output power. (**Right**) Spectral output FWHM variation with average output power. Insets show raw spectrometer data acquired at 800 nm and 1 mW (**left**) and 764 mW (**right**). All data was acquired from pulses propagating through 4 m of NCF.

the NCF we always ensured that the coupling of light into the fundamental mode was maximized by matching the size of focused spot to the modal field of fundamental mode at the input end of the fibre. Examples of the NCF output images at four discrete laser wavelengths are shown in Figure 3e. These images show no measureable multimodal component to the output of the fibre and so imply that light is guided via a single (fundamental) spatial mode.

3.3 Temporal and spectral pulse shape as function of transmitted average power

In Figure 4, the variation of temporal and spectral pulse widths at the NCF output as a function of average fibre output power at four distinct wavelengths is shown. Here 4 m of NCF was used. In all cases, there is less than 10% temporal and spectral broadening of the pulses as the average power is increased. The range of powers used for each data set was determined by the minimum output power that would still provide a measurable signal on the detector, and the maximum output power that was achievable with the laser source used for the measurement.

4. Two-photon microscopy using excitation pulses delivered via the NCF

Images from a freshly excised sample of mouse skin were acquired using our fibre-coupled multiphoton microscope that was reported in [20]. Briefly, the apparatus (shown in Figure 5) consists of a mode-locked Ti : Sapphire laser (Spectra Physics Mai Tai HP) which is fibre coupled by the NCF to a custom built laser scanning microscope. The microscope uses a scan and tube lens (Thorlabs LSM02-BB and AC508-100) to image a plane halfway between two closely spaced galvanometric mirrors (Camtech 6210H) onto the back focal plane of a water immersion microscope objective (Olympus UPLANSAPO60X). This allows the focused spot of the objective lens to be scanned across the field of view. Images are constructed by recording the multiphoton autofluorescence and SHG generated at each focused spot location that is coupled by a multimode fibre bundle to a photon multiplier tube (Becker & Hickl HPM-100-40). Note that no pre-chirp (dispersion compensation) unit is used in this apparatus, and no changes to the optical setup were required for imaging at different excitation wavelengths.

Multiphoton excitation images acquired from a freshly excised sample of mouse skin are presented in Figure 6. The images show the same region of the

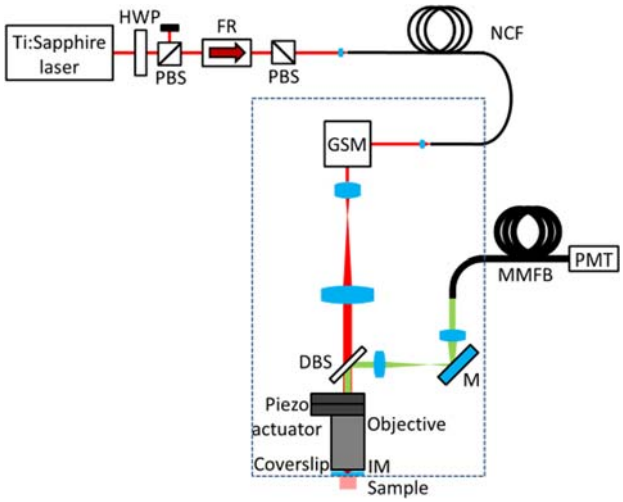

Figure 5 Schematic diagram of parts of the custom built fibre-coupled multiphoton microscope used to acquire autofluorescence images from *ex vivo* samples of mouse skin. DBS: 705 nm Dichroic beamsplitter; FR: Faraday rotator; GSM: Galvanometric scanning mirrors; HWP: Half waveplate; NCF: Negative curvature fibre; IM: Immersion media (water); M: Mirror; MMFB: Multimode fibre bundle; PBS: Polarising beamsplitter; PMT: Photon multiplier tube.

sample, imaged at two depths 25 μm apart, at four wavelengths (740 nm, 780 nm, 820 nm, 860 nm). Each image was acquired using 30 mW of average power at the sample, and an acquisition time of 30 s. The image in the top left hand corner of Figure 6 (upper layer imaged at 740 nm excitation) shows features consistent with NAD(P)H autofluorescence from cells in the epidermis (with characteristic dark cell nuclei) surrounded by thin lines of keratin autofluorescence caused by wrinkles in the skin surface. As the excitation wavelength is increased at this imaging depth (moving top-left to top-right in Figure 6) autofluorescence from keratin and what is likely to

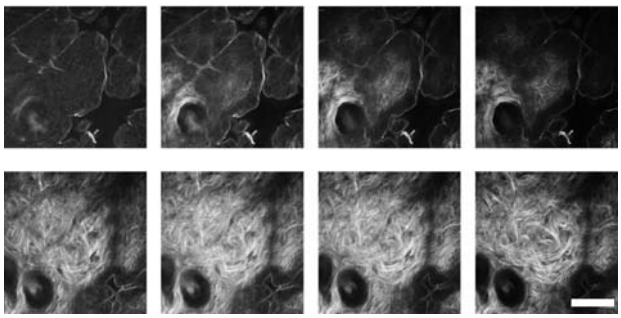

Figure 6 Multiphoton autofluorescence images of two planes of the epidermis of an *ex vivo* mouse skin sample. The top row shows the keratin layer, and the autofluorescence in the bottom row derives mostly from collagen and elastin. Each column is acquired at a different wavelength (left to right: 740 nm, 780 nm, 820 nm, 860 nm). Scale bar is 50 μm.

be a mixture of autofluorescence from elastin fibres and SHG from collagen becomes more pronounced relative to the cellular autofluorescence. In the bottom row acquired at a deeper depth, the signal detected is attributed mainly to collagen SHG and some autofluorescence of elastin. In the future it would be straightforward to discriminate collagen SHG and elastin autofluorescence by the addition of multiple spectral detection channels.

5. Conclusion

Multiphoton microscopy requires ultrashort optical pulses (<200 fs) incident at the sample. This pulse duration should be maintained over a broad wavelength range to allow a diverse range of fluorophores to be efficiently excited. The NCF reported herein is a promising candidate for flexible fibre coupled delivery of light for multiphoton and other nonlinear microscopy modalities. The NCF has a low attenuation (<0.3 dB m^{-1}) across a wavelength range of 600–850 nm that can be exploited when exciting fluorescence in commonly studied endogenous (NADH, Collagen, Elastin, FAD) and exogenous fluorophores. This attenuation compares favorably with figures reported for other inhibited guidance fibres [21]. Kagome type hollow core fibres have been manufactured with attenuation of 0.07 dB m^{-1} at 780 nm however the GVD of these fibres was not reported [22]. The NCF has a large 22 μm diameter core which reduces the impact of waveguide dispersion in the fibre whilst still allowing the fibre to guide in a single transverse spatial mode. The variation in group velocity dispersion in the NCF between 700 nm and 880 nm was measured to be <1600 fs^2 m^{-1}. No significant nonlinear temporal or spectral pulse broadening was observed when increasing the average laser power at the fibre output to the maximum achievable values (808 mW at 800 nm). Finally the NCF was used with a multiphoton microscope to deliver ultrashort pulses to excite autofluorescence and SHG in an *ex vivo* tissue sample. The images show features such as collagen fibrils with similar clarity to commercial free space systems [23], suggesting the NCF is well suited to excitation light delivery for nonlinear microscopy.

Acknowledgements This research was funded by a UK Engineering and Physical Sciences Research Council Healthcare Technologies Challenges for Engineering research grant (EP/K020102/1). The fibre used in these experiments was originally fabricated for EP/K03197X/1. PMWF and JK contributed equally to this work. The authors gratefully acknowledge expert assistance from Helen Goyal at Imperial CBS in providing and preparing the mouse skin samples.

References

[1] R. Wolleschensky, T. Feurer, R. Sauerbrey, and U. Simon, Appl. Phys. B. **67**, 87–94 (1998).
[2] F. Helmchen, M. S. Fee, D. W. Tank, and W. Denk, Neuron **31**, 903–912 (2001).
[3] D. Bird and M. Gu, J. Microsoc. **208**, 35–48 (2002).
[4] F. R. Cregan, B. J. Mangan, J. C. Knight, T. A. Birks, P. St. J. Russell, P. J. Roberts, and D. C. Allan, Science **285**, 1537–1539 (1999).
[5] S. Tai, M. Chan, T. Tsai, S. Guol, and L. Chen, C. Sun, Opt. Express **12**, 6122 (2004).
[6] D. Kim, K. Kim, S. Yazdanfar, and P. T. C. So, Proc. SPIE **5700**, 14–22 (2005).
[7] B. Flusberg, J. Jung, E. Cocker, E. P. Anderson, and M. J. Schnitzer, Opt. Lett. **30**, 2272–2274 (2005).
[8] L. Fu, A. Jain, H. Xie, C. Cranfield, and M. Gu, Opt. Express **14**, 1027–1032 (2006).
[9] C. J. Engelbrecht, R. S. Johnston, E. J. Seibel, and F. Helmchen, Opt. Express **16**, 5556–5564 (2008).
[10] M. G. Welch, C. E. de Nobriga, R. A. Correa, W. J. Wadsworth, and J. C. Knight, Opt. Express **17**, 9006–9011 (2009)
[11] F. Couny, F. Benabid, P. J. Roberts, P. S. Light, and M. G. Raymer, Science **318**, 1118–1121 (2007).
[12] P. St. J. Russel, P. Holzer, W. Chang, A. Abdolvand, and J. C. Travers, Nat. Photonics **8**, 278–286 (2014).
[13] J. Yu, H. Zeng, H. Lui, J. Skibina, G. Steinmeyer, and S. Tang, Opt. Express **22**, 10366–10379 (2014).
[14] W. Denk, J. Strickler, and W. Webb, Science **6**, 73–76 (1990).
[15] F. Yu and J. C. Knight, IEEE J. Sel. Topics Quantum Electron **22**, 1–10 (2016).
[16] F. Yu and J. C. Knight, Opt. Express **21**, 21466–21471 (2013).
[17] P. Jaworski, F. Yu, R. M. Carter, J. C. Knight, J. D. Shephard, and D. P. Hand, Opt. Express **23**, 8498–8506 (2015).
[18] C. Harvey, F. Yu, J. C. Knight, W. Wadsworth, and P. Almeida, CLEO **2015**, p. STh1L.5 (2015).
[19] H. Choi, P. T. C. So, Sci. Rep. **4**, 6626 (2014).
[20] B. Sherlock, S. Warren, J. Stone, M. Neil, C. Patterson, J. Knight, P. French, and C. Dunsby, Biomed. Opt. Express **6**, 1876–1884 (1015).
[21] J. S. Skibina, R. Iliew, J. Bethge, M. Bock, D. Fischer, V. I. Beloglasov, R. Wedell, and G. Steinmeyer, Nat. Photonics **2**, 679–683 (2008).
[22] T. D. Bradley, Y. Wang, M. Alharbi, B. Debord, C. Fourcade-Dutin, B. Beaudou, F. Gerome, and F. Benabid, J. Lightwave Technol. **31**, 2752–2755 (2013).
[23] X. Chen, O. Nadiarynkh, S. Plotnikov, and P. J. Campagnola, Nat. Protoc. **7**, 654–669 (2012).

The raw data associated with this paper can be found at http://dx.doi.org/10.5281/zenodo.45922 and the raw image data is available through Imperial College London's OMERO server at https://cisbic.bioinformatics.ic.ac.uk/omero/webclient/?show=dataset-8215.